PDB References: 3p7p; 3p7q; 3p7r; 3p7s; 3p7t; 3p7u; 3p7v; 3p7w.

Similarities and differences in radiation damage at 100 K *versus* 160 K in a crystal of thermolysin

Douglas H. Juers[a,b,c,d]* and Martin Weik[b,c,d,e]

[a]Department of Physics, Whitman College, Walla Walla, WA 99362, USA, [b]CEA, Institut de Biologie Structurale, F-38054 Grenoble, France, [c]CNRS, UMR5075, F-38027 Grenoble, France, [d]Université Joseph Fourier, F-38000 Grenoble, France, and [e]ESRF, 6 rue Jules Horowitz, BP 220, 38043 Grenoble Cedex, France. E-mail: juersdh@whitman.edu

The temperature-dependence of radiation damage in macromolecular X-ray crystallography is currently much debated. Most protein crystallographic studies are based on data collected at 100 K. Data collection at temperatures below 100 K has been proposed to reduce radiation damage and above 100 K to be useful for kinetic crystallography that is aimed at the generation and trapping of protein intermediate states. Here the global and specific synchrotron-radiation sensitivity of crystalline thermolysin at 100 and 160 K are compared. Both types of damage are higher at 160 K than at 100 K. At 160 K more residue types are affected (Lys, Asp, Gln, Pro, Thr, Met, Asn) than at 100 K (Met, Asp, Glu, Lys). The X-ray-induced relative atomic *B*-factor increase is shown to correlate with the proximity of the atom to the nearest solvent channel at 160 K. Two models may explain the observed correlation: either an increase in static disorder or an increased attack of hydroxyl radicals from the solvent area of the crystal.

Keywords: radiation damage; solvent channels; static disorder; radicals.

1. Introduction

Radiation damage to macromolecular crystals has been well studied at 100 K owing to intense interest in understanding and utilizing the processes occurring readily at third-generation synchrotron sources (for reviews, see Holton, 2009; Garman, 2010). Global effects from radiation exposure at this temperature include decreasing diffraction intensity, increasing the *B*-factor, increasing *R*-factors, often increasing mosaicity and increasing unit-cell volume. Damage has also been recorded at specific sites (Helliwell, 1988; Weik *et al.*, 2000; Burmeister, 2000; Ravelli & McSweeney, 2000) in several different proteins, and there is evidence that metalloproteins are readily reduced (Schlichting *et al.*, 2000; Berglund *et al.*, 2002; Adam *et al.*, 2004; Yano *et al.*, 2005; Beitlich *et al.*, 2007; Corbett *et al.*, 2007; Hough *et al.*, 2008) and that active-site residues are particularly sensitive (Weik, Ravelli *et al.*, 2001; Matsui *et al.*, 2002; Dubnovitsky *et al.*, 2005; Roberts *et al.*, 2005; Adam *et al.*, 2009).

The temperature dependence of radiation damage effects is now being studied (for a review, see Weik & Colletier, 2010), with a focus on temperatures below 100 K (Chinte *et al.*, 2007; Corbett *et al.*, 2007; Meents *et al.*, 2007, 2010; Petrova *et al.*, 2010). At lower temperatures the radiation damage effects occur at a higher dose than at 100 K, so to minimize damage effects there is some interest in collecting diffraction data below 100 K. A recent report suggested an optimum of ∼50 K (Meents *et al.*, 2010).

Work has also been carried out to understand damage above 100 K (Weik, Ravelli *et al.*, 2001; Ravelli *et al.*, 2002; Teng & Moffat, 2002; Borek *et al.*, 2007; Colletier *et al.*, 2008; Meents *et al.*, 2010; Warkentin & Thorne, 2010). In one example, increasing the temperature to 155 K enhanced specific damage occurring at 100 K, as well as opening up new sites of damage (Weik, Ravelli *et al.*, 2001). Conformational changes were observed at 155 K, suggesting an increase in flexibility in the protein at this temperature. Subsequent studies on other systems showed an increase in global radiation damage indicators at higher temperatures (Borek *et al.*, 2007; Meents *et al.*, 2010) and a dependence of the radiation-induced unit-cell volume change on temperature (Ravelli *et al.*, 2002; Borek *et al.*, 2007). From a crystal preservation perspective for the purpose of recording high-quality diffraction data, higher temperatures are to be avoided because the damage effects described above occur at a lower absorbed X-ray dose. However, increased mobility at higher temperatures has also been used in conjunction with radiation damage effects to elicit functional information by kinetically trapping intermediate states (Weik, Ravelli *et al.*, 2001; Colletier *et al.*, 2008). Additionally, specific radiation damage has been used to determine crystal structures by using single isomorphous replacement (SIR) or multiple isomorphous replacement (MIR) with pre- and post-damage data sets (Ravelli *et al.*, 2003).

Since relatively few systems have been studied for radiation damage effects above 100 K we set out to conduct a damage

experiment using a protein heretofore uncharacterized with respect to radiation damage. By monitoring atomic B-factor changes in a crystal of thermolysin exposed to high-intensity radiation, we find both similarities and differences in radiation damage at 100 K versus 160 K. At the higher temperature some sites of specific damage are the same, including methionine sulfurs and carboxylate groups, while other new sites of damage appear, including side-chain amides of asparagine and glutamine residues. The new damage sites tend to be closer to the solvent region of the crystal. This can be explained either by solvent-produced radical ions at 160 K, which damage the protein in a depth-dependent manner, or by development of rotational static disorder via structural re-arrangements from radiation-induced breaks in crystal contacts.

2. Materials and methods

2.1. Crystal preparation

Crystals of thermolysin from *Bacillus thermoproteolyticus* (Sigma-Aldrich, catalog #P1512) were grown using hanging-drop vapor diffusion (Hausrath & Matthews, 2002). The purchased protein was used without further preparation and dissolved at 100 mg ml^{-1} in 45% (v/v) DMSO. Drops were made by mixing 5 µL of this protein solution with 5 µL 35% (v/v) DMSO, and set up over 5% (v/v) saturated ammonium sulfate. Crystals in space group $P6_122$ grew in a few days. Approximately 1 d prior to data collection the crystals were transferred to sitting drops composed of 30% (v/v) ethylene glycol over a well solution of 30% ethylene glycol. The crystals were washed with 30% ethylene glycol a few times over a few hours to eliminate any residual DMSO.

2.2. X-ray data collection and processing

X-ray data were collected at beamline ID14-EH4 (McCarthy et al., 2009) at the European Synchrotron Radiation Facility. The aperture was set to give a beam with a rectangular cross section of 40 µm (horizontal) $\times$ 100 µm (vertical). The energy was set to 13.20 keV (0.9393 Å). A single crystal (a 250 µm-long hexagonal rod of diameter 100 µm with a uniform visual appearance along its length) was used for data collection. At each temperature four data sets were collected at 10% transmittance (i.e. the beam intensity was attenuated by 90% before interacting with the crystal). During a data set, composed of 50 frames (1° oscillation, exposure time 1 s per frame), a dose of 0.25 MGy was absorbed as calculated using the program *RADDOSE* (Paithankar et al., 2009). Between data sets, the crystal was exposed over the same total oscillation range but with 100% transmittance (i.e. the beam was unattenuated), corresponding to a dose of ∼2 MGy. After the exposures at 100 K the temperature was increased at a rate of 0.1 K s^{-1} to 160 K, the crystal was translated by 80 µm leaving a 40 µm gap of unexposed crystal material; the procedure was then repeated. The purpose of the 40 µm gap was to limit the diffusion of damaging species created during the 100 K exposures into the

zone of the crystal used for the 160 K exposures. At 100 K the penumbral radiation damage is limited to a few micrometers surrounding the area directly exposed to the X-ray beam (Holton, 2009). Since the experiment was carried out at 160 K, a gap considerably larger than a few micrometers was considered to be potentially necessary. After the data collection at 160 K, the temperature was increased to 240 K and the crystal was again translated by 80 µm. However, at 240 K the scattering pattern showed no Bragg diffraction spots. The temperature was controlled with an Oxford Cryosystems 700 system, and the warming rate was 0.1 K s^{-1}. *MOSFLM* (Leslie, 1992) and *SCALA* (Evans, 2006) were used to process all data to 2.2 Å resolution, with the resolution limit of the fourth data set at 160 K. *Truncate* was used to determine the Wilson B-factor (French & Wilson, 1978) and *SCALEIT* (Howell & Smith, 1992) to determine the relative isotropic B-factor between data sets.

The intensity decay was determined by calculating the total diffracted intensity (I_{tot}) for the data set from $\langle I \rangle$ and the total number of reflections as output from *SCALA* (Table 1; all data from 34 to 2.2 Å were used), and normalizing this to the first data set at each temperature. A plot of I_{tot} versus dose yields $D_{1/2}$, the dose at which I_{tot} drops by 1/2 (Owen et al., 2006). The B-factor decay was determined by calculating the B-factor relative to the first data set at each temperature (B_{rel}) using *SCALEIT*. The slope of a linear fit to B_{rel} versus D yields the coefficient of sensitivity, $s_{AD} = (\Delta B_{rel}/\Delta D)(1/8\pi^2)$ (Kmetko et al., 2006).

2.3. Structure refinement and analysis

For structure determination and refinement, rigid-body refinement was first performed on Protein Data Bank (PDB) entry 8tln against the first 100 K data set (hereafter called data set 100a) using *REFMAC* (Murshudov et al., 1997). Restrained positional and B-factor refinement followed using all data (less 5% reserved for R-free calculations), alternating with rounds of map inspection, model building, and water removal and addition using *Coot* (Emsley et al., 2010). This refined 100 K structure (structure 100a) was then used as the initial model for refinement against the seven other data sets, which were refined as above. The coordinates have been deposited in the PDB with accession codes 3p7p, 3p7q, 3p7r, 3p7s, 3p7t, 3p7u, 3p7v and 3p7w.

Structure analysis was carried out with *EDPDB* (Zhang & Matthews, 1995), *Coot*, *UCSF Chimera* (Pettersen et al., 2004), *MSMS* (Sanner et al., 1996) and programs written by one of the authors (DHJ). *EDPDB* was used to calculate B-factor changes, coordinate manipulations and structure overlays. *Coot*, *UCSF Chimera* and *PyMOL* (Schrödinger, San Diego, CA) were used for structure visualization and mapping atom properties (e.g. ΔB and d_{nc}) to coordinate positions. *MSMS* was used to calculate solvent-accessible surface areas and molecular volumes. The distance from each atom to the nearest solvent channel (d_{nc}) was determined as follows. First, the unit cell was divided into a three-dimensional rectangular grid with spacings of 1 Å. Grid points were assigned to

Table 1
Data collection and refinement statistics.

All data sets were processed from 34 to 2.2 Å and contained 17480 ± 140 reflections (2494 ± 20 in the high-resolution bin), with multiplicity of 5.6 (5.8 in the high-resolution bin). The statistics below are given for the whole data set with values for the high-resolution bin (2.31–2.20 Å) in parentheses. $\langle I \rangle$, $\langle I \rangle/\sigma(I)$, R_{meas} and N_{ref} (number of reflections) are taken from output from *SCALA*. Wilson-B is from *TRUNCATE*. B_{rel} is calculated as described in §2. Mosaicity is from *MOSFLM*. The dose was determined with *RADDOSE*. R-value and R-free are refined crystallographic R values from *REFMAC*. Shift/rotation gives the translational shift and rotation needed to align the coordinates with the coordinates from data set 100a, as determined with *EDPDB*. For the slope of ΔB versus d_{nc}, ΔB refers to the B-factor change from the previous structure (*e.g.* 100b versus 100a, 100c versus 100b), with the exception of 160a, in which case ΔB refers to 160a versus 100a.

| Data set	100a	100b	100c	100d	160a	160b	160c	160d
Unit cell (a, c, Å)	93.22, 128.61	93.26, 128.69	93.31, 128.73	93.35, 128.78	93.56, 128.94	93.75, 128.84	93.85, 128.74	93.94, 128.68
$\langle I \rangle$	3489 (1605)	3273 (1408)	2935 (1190)	2642 (931)	2997 (1345)	2421 (888)	1962 (602)	1462 (405)
$\langle I \rangle/\sigma(I)$	6.3 (7.3)	6.8 (7.4)	7.1 (6.9)	6.7 (5.7)	7.2 (8.3)	6.7 (6.2)	6.6 (4.2)	6.4 (2.7)
R_{meas} (%)	9.2 (9.8)	8.7 (10.0)	8.5 (11.4)	8.9 (14.3)	8.3 (8.3)	8.4 (12.5)	9.1 (19.1)	10.0 (30.0)
N_{ref}	17356 (2477)	17380 (2482)	17397 (2481)	17421 (2482)	17520 (2504)	17564 (2499)	17597 (2512)	17625 (2515)
Wilson-B (Å^2)	14.6	15.9	17.0	19.2	15.1	18.7	21.8	24.7
$\langle I \rangle/I_0$	1	0.94	0.84	0.76	1	0.81	0.65	0.52
B_{rel} (Å^2)	0	5.8	9.7	19.5	0	15.1	23.8	33.8
Mosaicity (°)	0.26	0.28	0.32	0.38	0.14	0.25	0.31	0.37
Cumulative dose (MGy)	0.1	2.5	4.9	7.2	0.1	2.4	4.8	7.1
Cumulative time (min)	0	10.5	17.3	24.8	38.5	44.4	50	55.4
R-value	0.149	0.146	0.144	0.146	0.146	0.145	0.146	0.153
R-free	0.211	0.206	0.202	0.203	0.205	0.199	0.202	0.210
$\langle B \rangle_{prot}$ (Å^2)	10.1	11.5	12.5	14.9	10.8	15.0	18.6	22.8
$\langle B \rangle_{wat}$ (Å^2) (# waters)	21.5 (332)	23.5 (320)	25.3 (312)	28.0 (293)	23.2 (357)	28.9 (307)	33.7 (294)	36.0 (258)
Shift (Å)	0.00	0.03	0.07	0.11	0.21	0.40	0.51	0.60
Rotation (°)	0.00	0.00	0.00	0.00	0.00	0.00	0.38	0.45
Slope of ΔB versus d_{nc} (Å)	–	−0.03	−0.06	−0.03	−0.02	−0.31	−0.19	−0.12

'solvent channels' based on a cut-off distance (4.5 Å): if a grid point was greater than the cut-off distance from every protein atom, it was assigned to 'solvent channels'. Second, distances between the atom of interest and all solvent channel grid points were calculated. The smallest such distance was assigned as the parameter d_{nc} for that atom. The basic result of the present work, which is that the change in refined atomic B-factor, ΔB, owing to radiation exposure is negatively correlated with d_{nc} at 160 K, was robust to this cut-off distance with values between 3 and 6 Å giving the same qualitative result. Correlation coefficients were calculated using *StatPlus* and Microsoft *Excel*.

Comparisons of our results with previously reported radiation damage experiments were carried out. The structures used were thermolysin (PDB codes 3do1/3do0), acetylcholinesterase (1qid/1qie), malate dehydrogenase (2j5k/2j5q) and human aldose reductase (3ghr/3ghs) at 100 K, and acetylcholinesterase (2vja/2vjb and 2vjc/2vjd) at 100 and 150 K.

3. Results

3.1. Global indicators

Global indicators (total diffracted intensity, Wilson B-factor, mosaicity and unit-cell volume) provide evidence for increased radiation damage at 160 K compared with 100 K (Table 1 and Fig. 1). Two global metrics for radiation sensitivity have been suggested, one based on the diffracted intensity ($D_{1/2}$ = the dose at which the total diffracting power of the crystal is reduced by 1/2; Owen *et al.*, 2006) and the other based on the change in B-factor with dose (Kmetko *et al.*, 2006). Here, at 100 K we find $D_{1/2} = 14$ MGy and $s_{AD} =$
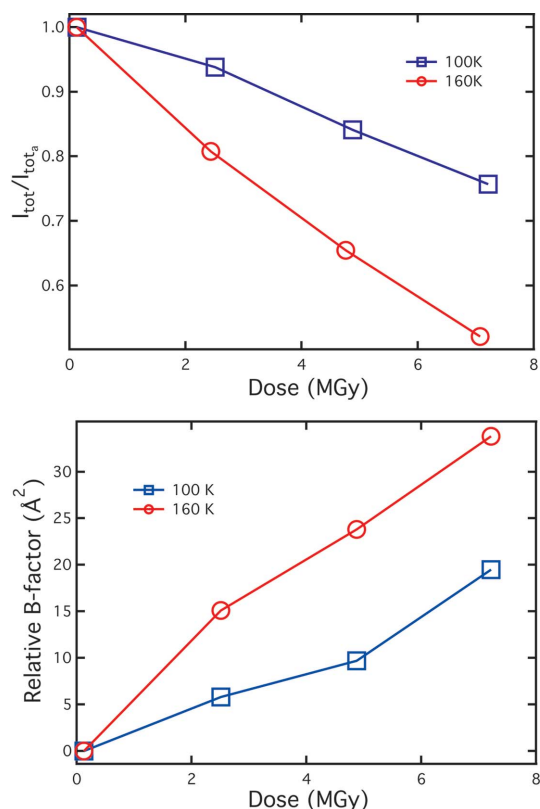
Figure 1
Progression of normalized average intensity (upper) and B-factor (lower) with dose. Lines connect successive points.

0.033 Å^2 MGy^{-1}, while at 160 K we find $D_{1/2} = 8.5$ MGy and $s_{AD} = 0.060$ Å^2 MGy^{-1}.

The mosaicity increased with dose at both temperatures studied (Fig. 2). Both the unit-cell volume and protein volume
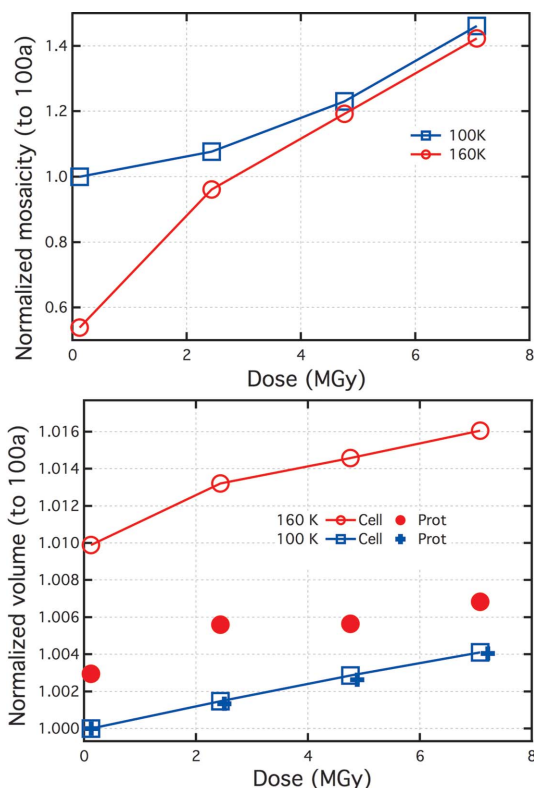
Figure 2
Dependence of mosaicity (upper), unit cell and molecular volumes (lower) on dose. Lines connect successive points. Mosaicity values are from *MOSFLM*. The molecular volume was determined using *MSMS*.

also increased with dose, at about the same rate for both temperatures (Fig. 2). However, the unit-cell volume increase at 160 K was anisotropic: one cell edge (*a*) increased while the other (*c*) decreased (Table 1).

3.2. Specific radiation damage

Specific radiation damage was initially investigated with difference Fourier maps, which showed some of the greatest susceptibility at sites normally expected to show specific damage. For example, of the top ten negative $F_o^{100b} - F_o^{100a}$ peaks (5 to 8σ; phases from the refined 100a structure) resulting from the first exposure at 100 K, two occur at the S$_\delta$ atoms of the two methionines in the structure and five occur at carboxylate O atoms (four aspartates and the carboxy terminus). Additionally, the four calcium ions and the active-site zinc ions showed negative features in the $F_o^{100b} - F_o^{100a}$ map.

The difference Fourier maps for the 160 K series and between the 100 and 160 K series were less easily interpreted, owing to non-isomorphism (Table 1). Many of the strongest map features were associated with shifts of atom positions. Consequently we turned to the refined structures to assess the effects of X-ray exposure.

Fig. 3 shows the relative susceptibility of different residue types in the structure by comparing the effect of radiation exposure on the refined *B*-factors to the overall *B*-factor change. At 100 K the most sensitive residues by this measure
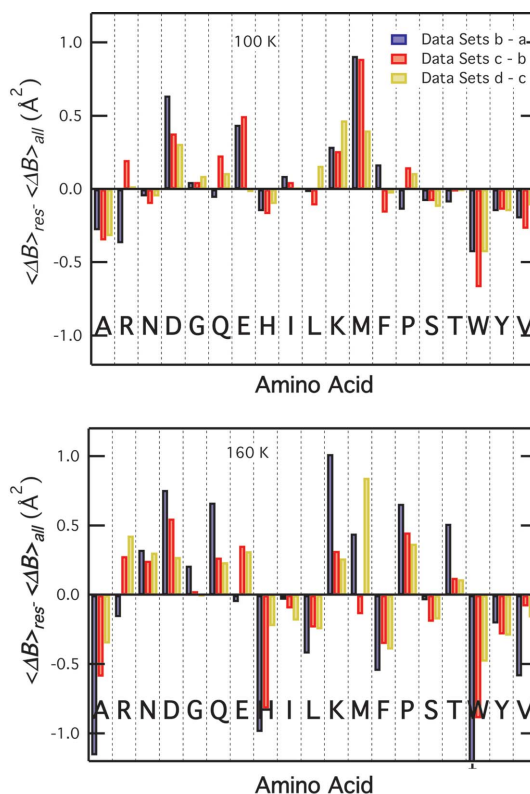
Figure 3
ΔB by residue type at 100 K (upper) and 160 K (lower). Positive values indicate that on average the residue undergoes a greater *B*-factor increase from radiation exposure than the rest of the structure. In the 160 K plot of data sets *b*–*a*, the value for tryptophan (-2.2 Å^2) is off the scale.

when comparing data sets *a* and *b* are Met, Asp, Glu and Lys in decreasing order (Fig. 3). Note that there are no cysteines and thus no disulfide bonds in thermolysin. At 160 K these residues are still susceptible, but others show similar susceptibilities (in decreasing order of *B*-factor change with exposure when comparing data sets *a* and *b*: Lys, Asp, Gln, Pro, Thr, Met, Asn). The metals sites have susceptibilities above average at 100 K. At 160 K the zinc has about average susceptibility, while the calcium ions become much more susceptible than average.

4. Discussion

4.1. Global damage indicators

The thermolysin crystals are radiation-sensitive at both 100 and 160 K. Using either the intensity decay ($D_{1/2}$) or *B*-factor decay (s_{AD}) the sensitivity is two to three times higher at 100 K than for apoferritin at 100 K (Owen *et al.*, 2006; Kmetko *et al.*, 2006). Also, using either measure, the thermolysin crystals roughly double in radiation sensitivity between 100 and 160 K, an increase similar to that reported for crystals of insulin (Meents *et al.*, 2010), glucose isomerase (Borek *et al.*, 2007) and thaumatin (Warkentin & Thorne, 2010) over the same temperature range.

We also examined unit-cell volume and mosaicity changes. Both the cell volume and protein volume show a comparable

response to radiation exposure: an expansion of 0.4–0.5% for 7 MGy, which is also similar at the two temperatures (Fig. 2). This contrasts with the response to only a change in temperature, in which the cell volume expands approximately three times more than protein volume between 100 and 160 K (*i.e.* comparing data sets 100*a* and 160*a*). The differential temperature response has been discussed and is related to differences between the thermal properties of the two types of materials comprising the crystal (protein *versus* bulk solvent; Juers & Matthews, 2001; Kriminski *et al.*, 2002).

The cause of the radiation-induced unit-cell volume expansion has been a matter of some debate (Ravelli *et al.*, 2002; Meents *et al.*, 2010; Warkentin & Thorne, 2010). Recently it has been proposed that the production of molecular hydrogen gas *via* the X-ray exposure of aliphatic groups expands the unit cell (Meents *et al.*, 2010). The similar magnitude of cell and protein volume expansion as a function of dose observed here suggests either (*a*) the production of hydrogen in equal concentrations in the two regions of the cell or (*b*) the rapid diffusion of hydrogen gas uniformly throughout the unit cell after its production. Although there are aliphatic groups in the bulk solvent [which is composed of 30% (*v/v*) ethylene glycol], their concentration should be higher in the protein. Therefore, the rapid diffusion model is favored here. Warkentin & Thorne, however, have noted that the diffusion of H_2 gas through amorphous ice at 100 K may be quite slow (*i.e.* ∼100 s to travel a distance of ∼25 water molecules; Warkentin & Thorne, 2010).

4.2. Specificity of damage: OH radicals *versus* electrons at 160 and 100 K

Previous observations of protein crystals at 100 K have shown radiation-susceptible sites to include disulfide bonds, carboxylate groups, tyrosine hydroxyls and methionine carbon–sulfur bonds (Weik *et al.*, 2000; Ravelli & McSweeney, 2000; Burmeister, 2000). The thermolysin crystals behave similarly, with methionine, aspartate and glutamate residues showing the highest radiation susceptibilities at 100 K. Note the absence of cysteine residues in thermolysin.

The detailed mechanisms of radical reactions as they relate to protein crystals have been investigated mainly using electron spin resonance (ESR) on model compounds, but are also now being studied with single-crystal spectrophotometry (Carpentier *et al.*, 2010). At the most basic level, X-ray radiation causes damage by ejecting electrons from atoms *via* the photoelectric effect or Compton scattering (primary damage; von Sonntag, 1987; Southworth-Davies *et al.*, 2007). These high-energy electrons then cause further ionizations (secondary damage). Possible species involved in secondary damage processes include electrons and holes, as well as other radicals that are produced in both the protein and solvent regions of the crystal. Radicals produced in the latter include radicals originating from water (solvated and aqueous electrons, H• and OH•) as well as from other components of the solvent (here mainly ethylene glycol).

At 77 K electrons appear to be mobile in proteins, travelling until they are trapped at electron sinks (Jones *et al.*, 1987), such as disulfide bonds (Symons, 1995) or, in their absence, side-chains with high electron affinity. Holes, however, are trapped prior to migrating long distances at peptide bonds *via* the loss of amide protons (Symons, 1995). Electrons and holes, as well as primary damage events, are likely to be responsible for the specific radiation damage observed at 100 K, which has been discussed previously (Ravelli & McSweeney, 2000; Burmeister, 2000). For example, disulfide breakage is thought to occur *via* electron capture, while decarboxylation of acidic side-chains is thought to proceed upon hole capture either from primary events or hole transfer. Some events at 100 K may be triggered by other species, for example thioether loss by methionine may occur *via* H-atom capture (Shimazu *et al.*, 1964).

At 160 K the irradiated thermolysin crystal has different characteristics than at 100 K. Approximately 98% of the protein atoms in the crystal were more radiation sensitive at 160 K than at 100 K. While the methionine sulfurs and carboxylate O atoms are still more sensitive than average, other sites (*e.g.* lysine, glutamine and proline, see Fig. 3) show equal or greater sensitivity. It appears, therefore, that the specificity of damage has changed somewhat between 100 and 160 K. One possible source of this new damage specificity is OH radicals produced in the solvent region of the crystal.

At 77 K the ESR spectrum of aqueous polethylene oxide is stable for several days and includes signals from OH radicals, which disappear upon warming to 115 K (Zakurdaeva *et al.*, 2005). Other experiments show the disappearance of radiation-induced OH radicals in ice in the range 90–130 K (Kroh *et al.*, 1961; Zakurdaeva *et al.*, 2005; Plonka *et al.*, 1984). The short lifetime of OH radicals at ∼130 K has been used to implement annealing processes for quenching OH radical signals in various low-temperature ESR experiments (Boon *et al.*, 1984). Other observations suggest that H radicals become mobile above 115 K (Fisher & Devlin, 1995; Southworth-Davies *et al.*, 2007; Garman & Nave, 2009). Therefore, we may expect that increasing the temperature of the thermolysin crystal to 160 K should significantly increase the damage activity of both OH and H radicals.

Hydroxyl radicals are powerful oxidizing agents, responsible for a variety of amino acid modifications (Xu & Chance, 2007; Davies & Dean, 1997), including deletions (*e.g.* decarboxylation of acidic side-chains) as well as, following subsequent reactions, additions of other moieties to the radical centers formed by H-atom abstraction. Also, the hydroxyl radical can itself add to aromatic rings and sulfur centers. Here, our metric for radiation damage is the increase in atomic *B*-factor, which will obviously be sensitive to deletion events. Addition events would be less likely produce *B*-factor increases unless, for example, they caused greater conformational disorder.

There are several known processes involving OH radicals consistent with our results at 160 K. Generally these are multistep processes involving first the creation of a radical somewhere on the side-chain *via* reaction with OH•, subsequent

reaction of this side-chain radical with molecular oxygen, and in some cases the breakdown of an unstable product (*e.g.* Arg, His, Cys; Xu & Chance, 2007). Owing to its hydrophobic nature, molecular oxygen should be available in the protein fraction of the crystal. These oxidation reactions result in guanidinium group loss by arginine (Ayala & Cutler, 1996; Xu *et al.*, 2003), decarboxylation of aspartate and glutamate (Davies *et al.*, 1995; Xu & Chance, 2004), main-chain breaks at proline residues (Dean *et al.*, 1989; Uchida *et al.*, 1990), loss of thioether from methionine (Hiller *et al.*, 1981; Xu & Chance, 2007), loss of the side-chain primary amine by lysine (Hawkins & Davies, 2001; Davies & Dean, 1997), and breakdown of acetamide (a model compound for asparagine and glutamine side-chain amides; Leitner *et al.*, 2002). These are all possible reactions that could become more active at higher temperatures, explaining the altered radiation susceptibility at 160 *versus* 100 K.

OH radicals are also indirectly responsible for addition reactions with most amino acids (see above), resulting in hydroxylation or carbonylation at many different sites on the side-chains (Xu & Chance, 2007). If a hydroxylation event were directed sterically to the same site on a particular side-chain on every protein molecule in the crystal, we would expect to see it as a positive peak in a difference map. Map inspection, however, showed no such peaks, suggesting low occupancy if such addition reactions are occurring. Addition reactions may be inhibited by steric constraints in the protein matrix, especially since the residues most sensitive to hydroxylation (*e.g.* Tyr, Phe) are among those most deeply buried in the protein. To the best of our knowledge, the current literature on radiation damage in protein X-ray crystallography does not contain evidence for radiation-induced additions in electron density maps.

4.3. The role of residue depth in protection from radiation damage

Previous investigations have demonstrated that there is no correlation between the solvent-accessibile surface of an atom and its radiation sensitivity at 100 K (Fig. 4) (Ravelli & McSweeney, 2000; Burmeister, 2000; Fioravanti *et al.*, 2007). The influence on radiation sensitivity of a related, yet distinct, parameter has not yet been addressed, *i.e.* of the distance of an atom to the nearest interphase between protein and solvent
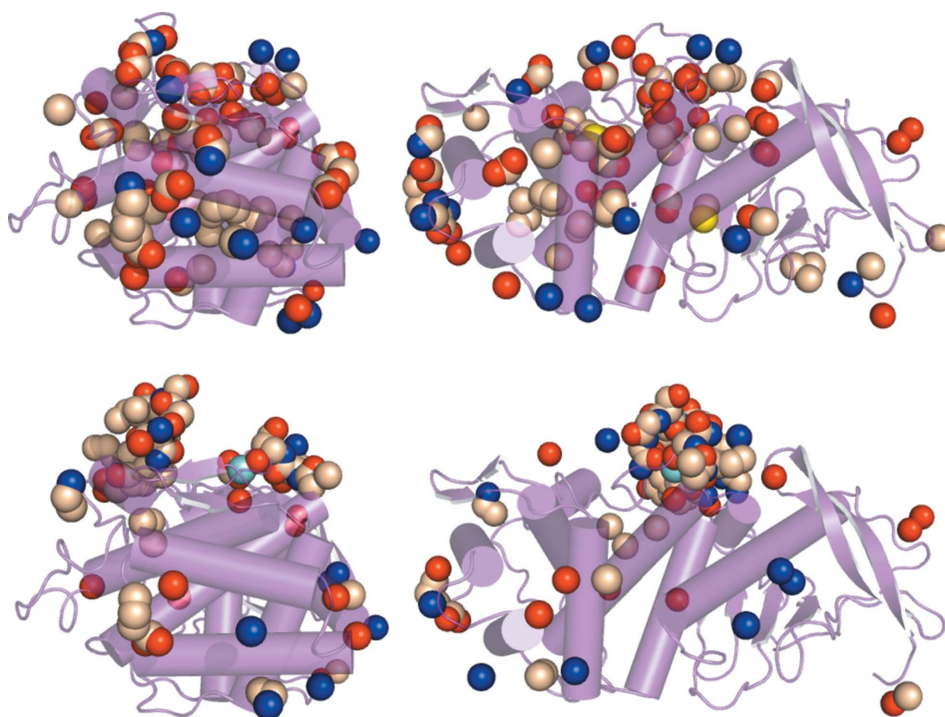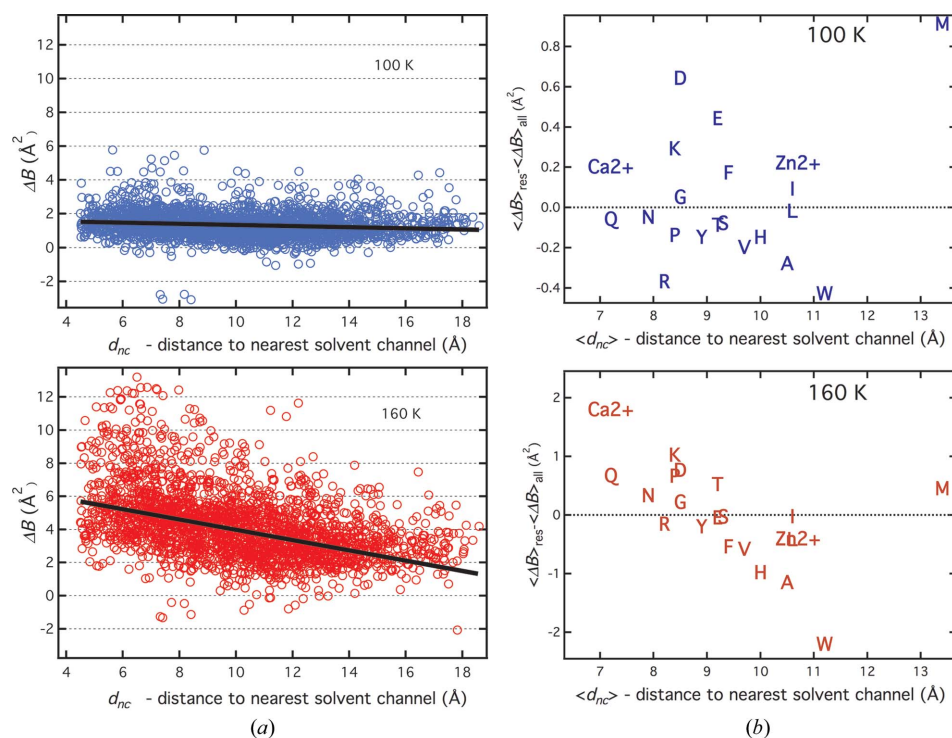

Figure 4
Backbone trace of the thermolysin molecule with the 130 atoms with the greatest *B*-factor increases shown with spheres (corresponding to ∼5% of the atoms in the protein; oxygen = red, nitrogen = blue, carbon = wheat, sulfur = yellow, calcium = cyan). At 100 K (upper; two orthogonal views of the molecule are shown) the 130 greatest *B*-factor increases are distributed evenly throughout the molecule, and include the two methionine S$_\delta$ atoms (yellow). In contrast, at 160 K (lower) they are biased towards the surface, and include a surface-exposed calcium ion (cyan). Figure prepared using *PYMOL*.

(referred to as depth hereafter). Since we are interested in the depth in the context of the crystalline protein, we determined the distance from the atom to the nearest solvent channel (d_{nc}), rather than to the surface of the protein in isolation. We then considered the correlation between the atom's dose-dependent ΔB and d_{nc} as a measure of the dependence of the radiation sensitivity on the proximity to the crystal solvent.

Fig. 5(*a*) shows ΔB *versus* d_{nc} for all atoms in the structure. The slopes of linear fits suggest the dependence of ΔB on d_{nc} is ten times greater at 160 K than 100 K for the first exposure (−0.31 *versus* −0.03 Å, Table 1). For the second and third exposures the slopes are −0.19 and −0.12 Å for 160 K, and −0.06 and −0.03 Å for 100 K, respectively. Thus, the effect persists but is less dramatic with later exposures.

The slopes of ΔB *versus* d_{nc} for thermolysin were compared with those for previously published radiation damage studies. There are several sets of refined protein structures in the PDB at increasing doses, most at 100 K. In one case, two structures of thermolysin before and after exposure at 100 K are given, although details of the work are unpublished and no dose information is given in the corresponding PDB entries (3do1/3do0). The slope of ΔB versus d_{nc} for this pair of structures is −0.09 Å, similar to our 100 K value of −0.03 Å. Other 100 K structures, *i.e.* acetylcholinesterase (Weik, Ravelli *et al.*, 2001; PDB codes 2vja/2vjb), malate dehydrogenase (Fioravanti *et al.*, 2007; PDB codes 2j5k/2j5q) and human aldose reductase (Petrova *et al.*, 2009; PDB codes 3ghr/3ghs) give slopes of

Figure 5
Dependence of ΔB for the first radiation exposure on proximity to solvent channels. (a) Plots of ΔB *versus* d_{nc} for each atom in the structure for 100 K (top) and 160 K (bottom). Linear fits to the data are in black. For the 100 K plot the correlation between ΔB and d_{nc} is -0.13 and the slope of the linear fit is -0.03 Å. At 160 K the correlation and slope become -0.44 and -0.31 Å, respectively. (b) ΔB *versus* d_{nc} averaged over each residue type. Between 100 K (top) and 160 K (bottom) the correlation between ΔB and d_{nc} improves significantly, from -0.23 to -0.81 (excluding methionine).

That the slope of ΔB with d_{nc} moves closer to zero with successive exposures would then indicate that this depth-dependent protection becomes less effective with greater doses. That is, the damage from the prior exposure diminishes the protective effect of the outer residues.

At 100 K both the zinc and calcium ions show greater than average susceptibility. At 160 K the Zn atoms show little change in their susceptibility, while the calcium ions display dramatically increased susceptibility. The zinc ion is ligated by two histidines and one glutamate; histidines tend to suffer less radiation damage than other residues and since they are ligating the zinc may offer this ion some protection. Both histidine and a zinc–alanyl–histidine complex (zinc carnosine) are known hydroxyl radical scavengers (Chan *et al.*, 1994; Yoshikawa *et al.*, 1991). Therefore, this active-site metal center may be naturally protected from OH radical damage. The calcium ions, on the other hand, are all ligated by O atoms from carboxylates, carbonyls or waters, groups known to be susceptible to damage. Damage to the calcium ligands could release the calcium from the protein, an event more likely to occur with greater solvent mobility that probably exists at 160 K (see below), since the calcium must be released to the bulk solvent.

-0.09, -0.12 and -0.19 Å for doses of 1, 3.3 and 2.0 MGy, respectively. In only one case, for acetylcholinesterase, are there data at both 100 K and a higher temperature. In this case the slope of ΔB *versus* d_{nc} was -0.10 Å at 100 K (dose = 7.0 MGy) and -0.26 Å at 150 K (dose = 6.5 MGy), an increase of $2.6\times$ over a similar temperature range to the experiment reported here, which is of the same order as our results, as follows. Using similar doses we calculate slopes of -0.12 Å at 100 K (100d *versus* 100a; dose of 7.2 MGy) and -0.62 Å at 160 K (160d *versus* 160a, dose of 7.1 MGy), a $5\times$ increase in the rate of change.

ΔB *versus* d_{nc} was considered on a residue basis. Fig. 5(b) shows graphs of ΔB *versus* d_{nc} averaged over all of the atoms in the crystal for each residue type. Excluding methionine, there is a much greater correlation at 160 K (correlation coefficient = -0.80) than at 100 K (correlation coefficient = -0.23). (Note that because deeper residues show smaller ΔB, correlation coefficients between ΔB and d_{nc} are negative.) In sum, the data show that on average the proximity of a residue to a solvent channel can predict ΔB at 160 K, but not at 100 K.

One way to explain the negative correlation of ΔB with d_{nc} at 160 K but not at 100 K is that at 160 K OH radicals produced in the solvent region of the crystal are no longer trapped, but free to diffuse and cause damage. The first residues they come into contact with should be those residues lining the solvent channels, so residues buried deeper inside the protein suffer less damage than those closer to the surface.

4.4. Solvent mobility and rotational static disorder

The negative correlation between ΔB and d_{nc} can also be explained simply *via* the creation of greater static disorder at 160 K, as opposed to being due to depth-dependent damage promoted by OH radicals released at a temperature between 100 and 160 K. Diffraction degradation from radiation exposure must involve the gradual misalignment of neighboring molecules. Random translational misalignments would cause increases in the B-factor which are uniform over all atoms. Random rotational misalignments would cause greater B-factor increases in atoms further from the average center of rotation. This could be more relevant at 160 K, where greater solvent mobility could allow for such movements more easily. The slope of ΔB *versus* d_{nc} at 160 K is approximately -0.3 Å. Given that the average radius of thermolysin is $\sim$25 Å, this means atoms on the surface show ΔB about 7.5 Å^2 greater than atoms in the center, which corresponds to 0.1 Å^2 in

atomic mean square displacement ($\langle u^2 \rangle$ using $B = 8\pi^2 \langle u^2 \rangle$). This corresponds to ~ 0.012 rad or $0.7°$ of greater angular disorder after radiation exposure than before. The decrease in slope of ΔB versus d_{nc} with successive exposures would then suggest that rotational misalignments contribute less to the static disorder as the exposures continue.

The solvent fraction of the crystal shows evidence of greater mobility at 160 K. The anisotropy in the cell volume changes at 160 K (Fig. 1), indicating that there is some reorientation of the molecule in the unit cell at 160 K (see also Table 1) which would require some redistribution of the bulk solvent molecules. Additionally, at 160 K, but not at 100 K, powder diffraction rings can be seen which are indicative of cubic ice formation, implying at least some of the bulk solvent has gone through the glass transition (Weik, Kryger *et al.*, 2001; Juers & Matthews, 2004; Kim *et al.*, 2009). The mosaicity showed considerable improvement in the region of the crystal used for the 160 K measurement, suggesting the initial cooling process produced some strain which was relieved with warming to 160 K, and produced a data set of slightly higher quality than at 100 K. (We cannot, however, exclude the possibility that this region of the crystal simply had lower intrinsic mosaicity than the region of the crystal used for the 100 K measurements.) This greater solvent mobility could facilitate the build-up of rotational disorder triggered by the degradation of crystal contacts by radical species, including newly available solvent-based radicals at 160 K.

At this point, neither of the above models can be eliminated. Both processes could be occurring. Distinguishing between them could be approached with higher-resolution data to permit simultaneous refinement of occupancy and B-factor, since the rotational disorder model would affect the B-factors but the solvent-produced radical model would affect mainly the occupancies. Another possibility might be to carry out mass spectrometric analysis after radiation exposure to identify the locations and types of damage events.

5. Conclusion

We have shown here that radiation effects at 160 K share some similarities and differences to those seen at 100 K. Upon warming the crystal to 160 K new amino acid residue types become susceptible in addition to those normally susceptible at 100 K. The newly susceptible residues tend to be closer to the protein crystal solvent channels. The data and analysis presented here are consistent with two models to explain this latter observation: (*a*) greater mobility and reactivity of radicals formed in the bulk solvent, in particular hydroxyl radicals, exacerbate secondary damage processes at 160 K, with residues buried more deeply in the protein being better protected from damage, and/or (*b*) static disorder induced by global radiation damage is greater at 160 K, owing to the greater mobility of the solvent system at this temperature.

References

Adam, V., Carpentier, P., Violot, S., Lelimousin, M., Darnault, C., Nienhaus, G. U. & Bourgeois, D. (2009). *J. Am. Chem. Soc.* **131**, 18063–18065.

Adam, V., Royant, A., Nivière, V., Molina-Heredia, F. P. & Bourgeois, D. (2004). *Structure*, **12**, 1729–1740.

Ayala, A. & Cutler, R. G. (1996). *Free Radical Biol. Med.* **21**, 65–80.

Beitlich, T., Kühnel, K., Schulze-Briese, C., Shoeman, R. L. & Schlichting, I. (2007). *J. Synchrotron Rad.* **14**, 11–23.

Berglund, G. I., Carlsson, G. H., Smith, A. T., Szöke, H., Henriksen, A. & Hajdu, J. (2002). *Nature (London)*, **417**, 463–468.

Boon, P. J., Cullis, P. M., Symons, M. C. R. & Wren, B. W. (1984). *J. Chem. Soc. Perkin Trans. 2*, pp. 1393–1399.

Borek, D., Ginell, S. L., Cymborowski, M., Minor, W. & Otwinowski, Z. (2007). *J. Synchrotron Rad.* **14**, 24–33.

Burmeister, W. P. (2000). *Acta Cryst.* D**56**, 328–341.

Carpentier, P., Royant, A., Weik, M. & Bourgeois, D. (2010). *Structure*, **18**, 1410–1419.

Chan, W. K. M., Decker, E. A., Lee, J. B. & Butterfield, D. A. (1994). *J. Agric. Food Chem.* **42**, 1407–1410.

Chinte, U., Shah, B., Chen, Y.-S., Pinkerton, A. A., Schall, C. A. & Hanson, B. L. (2007). *Acta Cryst.* D**63**, 486–492.

Colletier, J. P., Bourgeois, D., Sanson, B., Fournier, D., Sussman, J. L., Silman, I. & Weik, M. (2008). *Proc. Natl Acad. Sci. USA*, **105**, 11742–11747.

Corbett, M. C., Latimer, M. J., Poulos, T. L., Sevrioukova, I. F., Hodgson, K. O. & Hedman, B. (2007). *Acta Cryst.* D**63**, 951–960.

Davies, M. J. & Dean, R. T. (1997). *Radical-Mediated Protein Oxidation.* New York: Oxford University Press.

Davies, M. J., Fu, S. & Dean, R. T. (1995). *Biochem J.* **305**, 643–649.

Dean, R. T., Wolff, S. P. & McElligott, M. A. (1989). *Free Radic Res. Commun.* **7**, 97–103.

Dubnovitsky, A. P., Ravelli, R. B., Popov, A. N. & Papageorgiou, A. C. (2005). *Protein Sci.* **14**, 1498–1507.

Emsley, P., Lohkamp, B., Scott, W. G. & Cowtan, K. (2010). *Acta Cryst.* D**66**, 486–501.

Evans, P. (2006). *Acta Cryst.* D**62**, 72–82.

Fioravanti, E., Vellieux, F. M. D., Amara, P., Madern, D. & Weik, M. (2007). *J. Synchrotron Rad.* **14**, 84–91.

Fisher, M. & Devlin, J. P. (1995). *J. Phys. Chem.* **99**, 11584–11590.

French, S. & Wilson, K. (1978). *Acta Cryst.* A**34**, 517–525.

Garman, E. F. (2010). *Acta Cryst.* D**66**, 339–351.

Garman, E. F. & Nave, C. (2009). *J. Synchrotron Rad.* **16**, 129–132.

Hausrath, A. C. & Matthews, B. W. (2002). *Acta Cryst.* D**58**, 1002–1007.

Hawkins, C. L. & Davies, M. J. (2001). *Biochim. Biophys. Acta Bioenerg.* **1504**, 196–219.

Helliwell, J. R. (1988). *J. Cryst. Growth*, **90**, 259–272.

Hiller, K., Masloch, B., Goeble, M. & Asmus, K. (1981). *J. Am. Chem. Soc.* **103**, 2734–2743.

Holton, J. M. (2009). *J. Synchrotron Rad.* **16**, 133–142.

Hough, M. A., Antonyuk, S. V., Strange, R. W., Eady, R. R. & Hasnain, S. S. (2008). *J. Mol. Biol.* **378**, 353–361.

Howell, P. L. & Smith, G. D. (1992). *J. Appl. Cryst.* **25**, 81–86.

Jones, G. D., Lea, J. S., Symons, M. C. & Taiwo, F. A. (1987). *Nature (London)*, **330**, 772–773.

Juers, D. H. & Matthews, B. W. (2001). *J. Mol. Biol.* **311**, 851–862.

Juers, D. H. & Matthews, B. W. (2004). *Q. Rev. Biophys.* **37**, 105–119.

Kim, C. U., Barstow, B., Tate, M. W. & Gruner, S. M. (2009). *Proc. Natl Acad. Sci. USA*, **106**, 4596–4600.

Kmetko, J., Husseini, N. S., Naides, M., Kalinin, Y. & Thorne, R. E. (2006). *Acta Cryst.* D**62**, 1030–1038.

Kriminski, S., Caylor, C. L., Nonato, M. C., Finkelstein, K. D. & Thorne, R. E. (2002). *Acta Cryst.* D**58**, 459–471.

Kroh, J., Spinks, J. W. T. & Green, B. C. (1961). *J. Am. Chem. Soc.* **83**, 2201.

Leitner, N. K., Berger, P. & Legube, B. (2002). *Environ. Sci. Technol.* **36**, 3083–3089.

Leslie, A. G. W. (1992). *Joint CCP4 + ESF-EAMCB Newsl. Protein Crystallogr.* **26**.

McCarthy, A. A., Brockhauser, S., Nurizzo, D., Theveneau, P., Mairs, T., Spruce, D., Guijarro, M., Lesourd, M., Ravelli, R. B. G. & McSweeney, S. (2009). *J. Synchrotron Rad.* **16**, 803–812.

Matsui, Y., Sakai, K., Murakami, M., Shiro, Y., Adachi, S., Okumura, H. & Kouyama, T. (2002). *J. Mol. Biol.* **324**, 469–481.

Meents, A., Gutmann, S., Wagner, A. & Schulze-Briese, C. (2010). *Proc. Natl Acad. Sci. USA*, **107**, 1094–1099.

Meents, A., Wagner, A., Schneider, R., Pradervand, C., Pohl, E. & Schulze-Briese, C. (2007). *Acta Cryst.* D**63**, 302–309.

Murshudov, G. N., Vagin, A. A. & Dodson, E. J. (1997). *Acta Cryst.* D**53**, 240–255.

Owen, R. L., Rudiño-Piñera, E. & Garman, E. F. (2006). *Proc. Natl Acad. Sci. USA*, **103**, 4912–4917.

Paithankar, K. S., Owen, R. L. & Garman, E. F. (2009). *J. Synchrotron Rad.* **16**, 152–162.

Petrova, T., Ginell, S., Mitschler, A., Kim, Y., Lunin, V. Y., Joachimiak, G., Cousido-Siah, A., Hazemann, I., Podjarny, A., Lazarski, K. & Joachimiak, A. (2010). *Acta Cryst.* D**66**, 1075–1091.

Petrova, T., Lunin, V. Y., Ginell, S., Hazemann, I., Lazarski, K., Mitschler, A., Podjarny, A. & Joachimiak, A. (2009). *J. Mol. Biol.* **387**, 1092–1105.

Pettersen, E. F., Goddard, T. D., Huang, C. C., Couch, G. S., Greenblatt, D. M., Meng, E. C. & Ferrin, T. E. (2004). *J. Comput. Chem.* **25**, 1605–1612.

Plonka, A., Szajdzinskapietek, E. & Kroh, J. (1984). *Radiat. Phys. Chem.* **23**, 583–587.

Ravelli, R. B., Leiros, H. K., Pan, B., Caffrey, M. & McSweeney, S. (2003). *Structure*, **11**, 217–224.

Ravelli, R. B. & McSweeney, S. M. (2000). *Structure*, **8**, 315–328.

Ravelli, R. B. G., Theveneau, P., McSweeney, S. & Caffrey, M. (2002). *J. Synchrotron Rad.* **9**, 355–360.

Roberts, B. R., Wood, Z. A., Jönsson, T. J., Poole, L. B. & Karplus, P. A. (2005). *Protein Sci.* **14**, 2414–2420.

Sanner, M. F., Olson, A. J. & Spehner, J. C. (1996). *Biopolymers*, **38**, 305–320.

Schlichting, I., Berendzen, J., Chu, K., Stock, A. M., Maves, S. A., Benson, D. E., Sweet, R. M., Ringe, D., Petsko, G. A. & Sligar, S. G. (2000). *Science*, **287**, 1615–1622.

Shimazu, F., Kumta, U. S. & Tappel, A. L. (1964). *Radiat. Res.* **22**, 276–287.

Sonntag, C. von (1987). *The Chemical Basis of Radiation Biology.* New York: Taylor and Francis.

Southworth-Davies, R. J., Medina, M. A., Carmichael, I. & Garman, E. F. (2007). *Structure*, **15**, 1531–1541.

Symons, M. C. R. (1995). *Radiat. Phys. Chem.* **45**, 837–845.

Teng, T.-Y. & Moffat, K. (2002). *J. Synchrotron Rad.* **9**, 198–201.

Uchida, K., Kato, Y. & Kawakishi, S. (1990). *Biochem. Biophys. Res. Commun.* **169**, 265–271.

Warkentin, M. & Thorne, R. E. (2010). *Acta Cryst.* D**66**, 1092–1100.

Weik, M. & Colletier, J.-P. (2010). *Acta Cryst.* D**66**, 437–446.

Weik, M., Kryger, G., Schreurs, A. M. M., Bouma, B., Silman, I., Sussman, J. L., Gros, P. & Kroon, J. (2001). *Acta Cryst.* D**57**, 566–573.

Weik, M., Ravelli, R. B., Kryger, G., McSweeney, S., Raves, M. L., Harel, M., Gros, P., Silman, I., Kroon, J. & Sussman, J. L. (2000). *Proc. Natl Acad. Sci. USA*, **97**, 623–628.

Weik, M., Ravelli, R. B., Silman, I., Sussman, J. L., Gros, P. & Kroon, J. (2001). *Protein Sci.* **10**, 1953–1961.

Xu, G. & Chance, M. R. (2004). *Anal. Chem.* **76**, 1213–1221.

Xu, G. & Chance, M. R. (2007). *Chem. Rev.* **107**, 3514–3543.

Xu, G., Takamoto, K. & Chance, M. R. (2003). *Anal. Chem.* **75**, 6995–7007.

Yano, J., Kern, J., Irrgang, K. D., Latimer, M. J., Bergmann, U., Glatzel, P., Pushkar, Y., Biesiadka, J., Loll, B., Sauer, K., Messinger, J., Zouni, A. & Yachandra, V. K. (2005). *Proc. Natl Acad. Sci. USA*, **102**, 12047–12052.

Yoshikawa, T., Naito, Y., Tanigawa, T., Yoneta, T. & Kondo, M. (1991). *Biochim. Biophys. Acta*, **1115**, 15–22.

Zakurdaeva, O. A., Nesterov, S. V. & Feldman, V. I. (2005). *High Energy Chem.* **39**, 201–206.

Zhang, X.-J. & Matthews, B. W. (1995). *J. Appl. Cryst.* **28**, 624–630.